# Step-Edge-Guided Nucleation and Growth of Aligned $WSe_2$ on Sapphire *via* a Layer-over-Layer Growth Mode

Liang Chen, Bilu Liu,* Mingyuan Ge, Yuqiang Ma, Ahmad N. Abbas, and Chongwu Zhou*

Department of Electrical Engineering, University of Southern California, Los Angeles, California 90089, United States

**ABSTRACT** Two-dimensional (2D) materials beyond graphene have drawn a lot of attention recently. Among the large family of 2D materials, transitional metal dichalcogenides (TMDCs), for example, molybdenum disulfides ($MoS_2$) and tungsten diselenides ($WSe_2$), have been demonstrated to be good candidates for advanced electronics, optoelectronics, and other applications. Growth of large single-crystalline domains and continuous films of monolayer TMDCs has been achieved recently. Usually, these TMDC flakes nucleate randomly on substrates, and their orientation cannot be controlled. Nucleation control and orientation control are important steps in 2D material growth, because randomly nucleated and orientated flakes will form grain boundaries when adjacent flakes merge together, and the formation of grain boundaries may degrade mechanical and electrical properties of as-grown materials. The use of single crystalline substrates enables the alignment of as-grown TMDC flakes via a substrate—flake epitaxial interaction, as demonstrated recently. Here we report a step-edge-guided nucleation and growth approach for the aligned growth of 2D $WSe_2$ by a chemical vapor deposition method using C-plane sapphire as substrates. We found that at temperatures above 950 °C the growth is strongly guided by the atomic steps on the sapphire surface, which leads to the aligned growth of $WSe_2$ along the step edges on the sapphire substrate. In addition, such atomic steps facilitate a layer-over-layer overlapping process to form few-layer $WSe_2$ structures, which is different from the classical layer-by-layer mode for thin-film growth. This work introduces an efficient way to achieve oriented growth of 2D $WSe_2$ and adds fresh knowledge on the growth mechanism of $WSe_2$ and potentially other 2D materials.

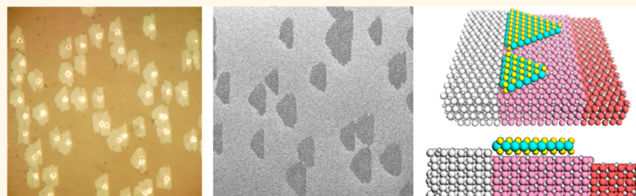

**KEYWORDS:** tungsten diselenides · transition metal dichalcogenides · TMDCs · chemical vapor deposition · sapphire · aligned growth · layer-over-layer

Layered two-dimensional (2D) materials beyond graphene such as transitional metal dichalcogenides (TMDCs),[1−3] black phosphorus (BP),[4−6] and silicene[7] recently have attracted significant attention due to their unique properties. A common feature shared by all 2D materials is that they possess weak interlayer interaction and strong intralayer covalent bonds, which makes them inherently flexible and good candidates for flexible electronics,[8−10] optoelectronic,[11−15] and some other applications.[2,3,16−21] So far, over tens of materials have been distinguished in this large family of 2D materials.[22] Among them, layered TMDCs are quite attractive because they have very diverse properties spanning metals, semiconductors, superconductors, *etc.*[2] Up to now, researchers have developed several methods including mechanical exfoliation,[23,24] liquid exfoliation,[25−27] chemical vapor deposition (CVD),[28−36] and physical vapor deposition (PVD)[37] to prepare monolayer or few-layer TMDC materials. Among these methods, vapor-phase-based growth approaches such as CVD and PVD are particularly interesting since they can produce materials with high quality and have the potential to be scaled up. Controlled growth of large single crystals and continuous thin films of $MoS_2$, $MoSe_2$, $WS_2$, and $WSe_2$ has been achieved recently.[28,31,38−41]

Location- and orientation-controlled growth of 2D TMDCs is another important direction to pursue in order to extract more potential from these materials. Currently, in many synthesis approaches, TMDC materials nucleate randomly on substrates, and their orientation cannot be well controlled. Misoriented growth can lead to the formation of grain boundaries and defects during the merging of adjacent domains, which may have negative effects on the electrical, optical, thermal, and mechanical properties of as-grown materials. For graphene growth, it has been shown that wafer-scale single-crystalline

* Address correspondence to chongwuz@usc.edu, biluliu@usc.edu.

Received for review May 20, 2015 and accepted July 21, 2015.

Published online July 29, 2015
10.1021/acsnano.5b03043

© 2015 American Chemical Society

graphene can be grown if the initial graphene nuclei have the same orientation, demonstrating the importance of alignment of graphene domains on large single crystal growth.[42] Recently, there have been a few attempts on the location- and orientation-controlled growth of TMDCs, especially $MoS_2$. For example, Han *et al*. have achieved location-controlled growth of $MoS_2$ *via* selective positioning of seeds.[43] In other studies, Dumcenco *et al.* and Ji *et al.* also demonstrated orientation-controlled growth of $MoS_2$ *via* a lattice epitaxial process on certain substrates.[44,45] Meanwhile, epitaxial growth of $WSe_2$ with alignment was also reported by Eichfeld *et al.* and Huang *et al.* using sapphire as substrates.[28,30] It was concluded that the interaction between TMDCs and crystalline sapphire substrates was the origin for the aligned growth. We noted that in these experiments the temperatures of the growth substrates were relatively low (700−800 °C). Here we report a new mechanism, step-edge-guided growth, for the aligned growth of $WSe_2$ on crystalline C-plane sapphire substrates at high temperatures above 950 °C. The idea was inspired by early studies on one-dimensional (1D) carbon nanotube[46−48] and nanowire growth,[49] where crystalline substrates with lattice-potential-guided or step-edge-guided growth are two major principles responsible for the aligned growth of these 1D systems. In this study, we found that the steps on the C-plane sapphire surface play a crucial role in oriented nucleation, directed propagation, and few-layer formation of $WSe_2$. We observed that such step-edge-guided aligned growth of $WSe_2$ flakes becomes prominent only at high growth temperatures due to the remarkable surface reconstruction of sapphire steps, which can only be trigged at high temperatures.[50,51] Moreover, we proposed that the growth of few-layer $WSe_2$ follows a novel layer-over-layer (LOL) growth mode, which is different from the classical layer-by-layer (LBL) growth mode as widely adopted in literature for thin-film growth.[52] Our finding opens up a possible way for location-controlled nucleation and orientation-controlled growth of 2D $WSe_2$ and potentially other TMDCs.

## RESULTS AND DISCUSSION

We used a CVD method to grow $WSe_2$ flakes, where selenium powders and $WO_3$ powders were used as source materials (see Methods section for experiment details). We have tested different substrates and growth temperatures and found that they have a significant influence on the features of as-grown $WSe_2$ flakes. Figure 1a, b, and c are optical microscopy images showing critical differences in the morphology of $WSe_2$ flakes after CVD growth at different temperatures on C-plane sapphire (Figure 1a and b) and Si/$SiO_2$ (silicon substrate with a 300 nm thick thermally grown $SiO_2$ layer, Figure 1c) substrates. The flakes in Figure 1a were synthesized on C-plane sapphire at 900 °C, which

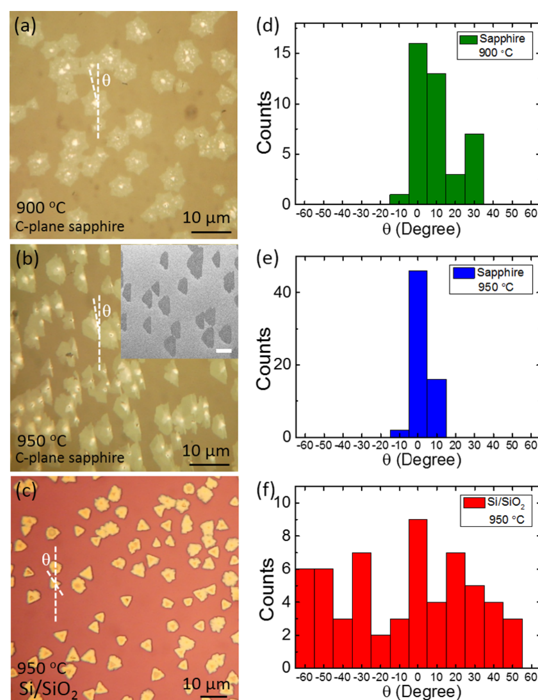


**Figure 1. Optical microscopic observations of $WSe_2$ flakes grown at different temperatures on C-plane sapphire and Si/$SiO_2$ substrates. (a and b) Optical microscopy images of aligned $WSe_2$ flakes grown on C-plane sapphire at 900 °C (a) and 950 °C (b). Inset in image (b) shows an SEM image of the sample grown at 950 °C. The scale bar is 10 $\mu$m. (c) Optical microscopy image of the $WSe_2$ flakes grown on Si/$SiO_2$ substrates at 950 °C. (d, e, and f) Histograms of the orientation distributions based on the images (a), (b), and (c), respectively. Growth on C-plane sapphire exhibits better orientation control than growth on Si/$SiO_2$ substrates (plots d and e *versus* plot f). Meanwhile, high growth temperature improves the alignment of $WSe_2$ growth on sapphire (plot d *versus* plot e).**

shows quasi-hexagonal shapes with certain preferred orientations, indicating a possible epitaxial growth process. Similar results have also been reported in CVD growth of graphene.[53] When the growth temperature increased to 950 °C, the as-grown flakes turned out to be trapezoids (which can also be described as truncated triangles) with a clear alignment of the base edges, as reveled by optical microscopy (Figure 1b) and scanning electron microscopy (SEM) imaging (inset of Figure 1b and Supporting Information Figure S1). Meanwhile, these flakes grown on C-plane sapphire are few-layer $WSe_2$ based on color contrast, as also revealed by atomic force microscopy (AFM) and Raman measurements shown later. In contrast, the flakes grown on a Si/$SiO_2$ substrate, under identical growth conditions, are mostly thick ones with a yellow color (Figure 1c). More importantly, a quick examination of the $WSe_2$ flakes grown on Si/$SiO_2$ indicates a random distribution of orientations of flakes compared to the samples grown on C-plane sapphire. We defined $\theta$, the smallest angle between the vertical direction in the images (which is close to the $[11\bar{2}0]$ direction for C-plane sapphire) and the diagonal (Figure 1a), the base edge (Figure 1b), and the midperpendicular line (Figure 1c), respectively, to

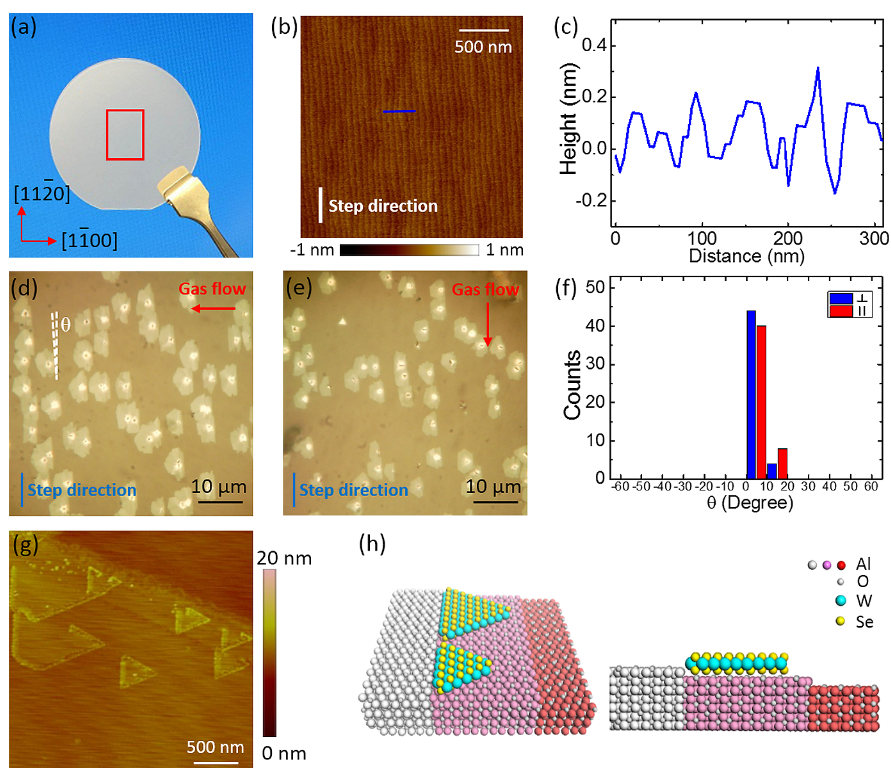


**Figure 2. Characterization of C-plane sapphires and observations of the step-edge-guided nucleation and aligned growth phenomena. (a) Photo image of commercial C-plane sapphire used in the experiments. (b) AFM height image of the sapphire surface after a high-temperature treatment (950 °C), revealing the formation of periodical step patterns. (c) Cross-section height profile of the steps along the blue line in (b). (d and e) Optical microscopy images of the as-grown $WSe_2$ flakes when the gas flow direction is perpendicular (d) or parallel (e) to the step direction during the growth. $\theta$ is defined as the angle between the step direction and the base edge of trapezoid flakes. (f) Statistical analysis of the alignment in (d) and (e) based on the $\theta$ values, showing good alignment in both experiments. (g) AFM image showing initial $WSe_2$ nuclei aligned at the sapphire step edges. (h) Atomic models illustrating the aligned nucleation of $WSe_2$ on C-plane sapphire.**

quantitatively describe the degree of alignment of each flake, as indicated in Figure 1a–c. The results are plotted in Figure 1d, e, and f, respectively, and several trends can be clearly observed. First, C-plane sapphire exhibits much better orientation control of as-grown $WSe_2$ flakes than $Si/SiO_2$ substrates do. Second, a high growth temperature improves the alignment of the $WSe_2$ flakes. For example, the flakes grown at 950 °C on C-plane sapphire show the best alignment, with 82% of the flakes having a $\theta$ less than 10° compared with the sample grown at 900 °C on sapphire. We also noted that the $WSe_2$ flakes grown at 950 °C in this study show one preferred alignment direction, which is parallel to the step edge direction of the sapphire substrates, as will be discussed later. In contrast, the $MoS_2$ flakes grown at 700 °C *via* a lattice epitaxial process in Kis *et al.*'s recent study show three preferred alignment directions.[44]

The aligned growth of $WSe_2$ flakes at 950 °C is likely to originate from atomic step edges on the C-plane sapphire substrates. Commercial C-plane sapphire wafers would usually develop atomic step-terrace structures on the surface when heated to high temperatures. Such atomic steps have been reported to have significant effects on the aligned growth of carbon nanotubes,[46−48] GaN nanowires,[49] and graphene.[54]

A photo image of the sapphire substrates used in this study is shown in Figure 2a, with a primary cutting edge of the (11$\bar{2}$0) plane. Thus, the direction parallel to the cutting edge is [1$\bar{1}$00], and the direction perpendicular to the edge is [11$\bar{2}$0]. Careful AFM characterization (Figure 2b and c) clearly shows the formation of atomic steps with a periodically distributed pattern appearing on the sapphire surface after the substrate went through a 950 °C pretreatment in an $Ar/H_2$ atmosphere (but without a $WO_3$ and Se source added during the pretreatment). Interestingly, such sharp steps are formed only at high temperatures above 950 °C due to the high-temperature-trigged surface reconstruction of sapphire substrates.[50,51] Without the high-temperature treatment, there are only irregular and isolated small steps (Supporting Information Figure S2), which is not sufficient to conduct step-edge-guided aligned growth of $WSe_2$ flakes. Extracted from the height profile (Figure 2c), the average terrace width is about 60 nm and the typical step height is around 0.2 nm ($c$/6, where $c$ = 12.99 Å is the lattice constant in the $z$-direction of C-plane sapphire). Those measured values are consistent with those reported in previous literature.[50,51] On the basis of the terrace width and step height, the corresponding miscut angle

was calculated to be 0.2°. This number is consistent with the datasheet from the vendor (University Wafers, USA). Moreover, these atomic steps are along the [11$\bar{2}$0] direction of the sapphire substrates. For convenience, we define it as the step direction in this study.

In 1D carbon nanotube growth, it has been well documented that both gas flow and substrate have effects on the morphology of the final products. By careful control of these two factors, complicated nanotube structures such as serpentine nanotubes have been grown.[55,56] It would be interesting to study whether such effects would happen in 2D material growth as well. To further study the alignment mechanism and particularly the effect of sapphire steps on the aligned growth of $WSe_2$ flakes, controlled experiments were conducted by changing the gas flow direction with respect to the sapphire step direction. The gas flow direction is perpendicular to the step direction in Figure 2d, while the gas flow direction is parallel to the step direction in Figure 2e. From optical microscopic observations, the as-grown flakes on both samples are all aligned with the step direction regardless of the change of gas flow directions. These results confirm that the alignment indeed originates from the substrate steps, not from gas flow. A statistical analysis of the degree of alignment based on Figure 2d and e is also performed and presented in Figure 2f. The angles between the step direction and the base edge of the trapezoid flakes were measured to verify the alignment. Among 48 flakes we examined in Figure 2d, 44 of them are well aligned with an angle less than 10°. The result on the other sample in Figure 2e is similar to the sample in Figure 2d; specifically, 40 flakes out of a total of 48 flakes are aligned with an angle less than 10°. On the basis of the above experiments, we conclude that sapphire steps are responsible for the aligned growth of $WSe_2$ flakes, and good alignment can be achieved through careful engineering of those atomic steps.

In-depth AFM studies further reveal that the aligned growth of $WSe_2$ flakes originates from the preferred nucleation of $WSe_2$ nuclei along the atomic steps on sapphire surface. In our experiments, we observed the initial nuclei are formed along the step edges with the same orientation as shown in Figure 2g and Figure S3 (Supporting Information). We speculate that the step edges on sapphire substrates are more attractive to reactants than other portions of the substrate at the initial $WSe_2$ nucleation stage because of the existence of dangling bonds and defects at these step edges.[57] In chemical reactions, atoms or molecules of reactants would choose sites of the highest bonding energy and preferentially absorb at those positions. Usually, defect sites such as steps on a flat surface have the highest binding energy, and therefore, the atomic steps of materials are generally more reactive than atomically flat areas. We speculate that this might be the major reason for the preferential nucleation of $WSe_2$ nuclei close to the atomic steps of sapphire, as observed in this study. In addition, nucleation of $WSe_2$ at atomic steps of sapphire can increase the contact areas and, consequently, the strength of van der Waals interactions between $WSe_2$ and the substrate. This will help stabilize the small nuclei of $WSe_2$ especially at the initial nucleation stage. Consequently, step edges can serve as active sites for $WSe_2$ nucleation and subsequent growth. A similar effect has also been reported in carbon nanotube growth.[46] Meanwhile, as Wang *et al.* mentioned in previous $MoS_2$ growth work, Mo atoms and S atoms have different chemical activities, which would be similar for the different binding energies here between sapphire step edges and W or Se atoms or species.[58] Thus, it is possible that one kind of element between W and Se may preferentially adsorb at the step edges of sapphire. Figure 2h shows relevant atomic models to describe such step-edge-guided nucleation and aligned growth of $WSe_2$ flakes. The gas phase reactants during the CVD $WSe_2$ growth would preferentially attach to the step edges, form initial aligned $WSe_2$ nuclei, and further merge into flakes, which would also be aligned along the step edges.

The as-grown flakes on sapphire were characterized to be few-layer $WSe_2$ by Raman and AFM. Figure 3a shows a typical $WSe_2$ flake with a trapezoid shape, and the size of this flake is around 10 $\mu$m. Two characteristic Raman peaks of $WSe_2$ at 247 and 256 $cm^{-1}$, corresponding to $E^1_{2g}$ and $A_{1g}$ modes, were observed in the Raman spectrum (Figure 3b). Meanwhile, another sharp peak at around 306 $cm^{-1}$ assigned to the $B^1_{2g}$ mode also exists, suggesting the formation of few-layer $WSe_2$, as this $B^1_{2g}$ peak is quite sensitive to the layer numbers of $WSe_2$.[23] Later, we performed Raman intensity mapping (Figure 3c) on the flake to study the structural uniformity. Interestingly, the mapping results reveal that the Raman intensity at 247 $cm^{-1}$ has some variation across the flake. Specifically, in the mapping image, the intensity in the front area and that in the area along the base edge are different. More Raman measurements on other flakes show similar results (Supporting Information Figure S4). Such variation in Raman signal comes from the variation of thickness, which is also revealed by AFM studies later.

Detailed AFM measurements are shown in Figure 3d, e, g, and h, revealing the fine structures of the same trapezoid flake as well as its presence on a stepped sapphire substrate. Figure 3d is an AFM height image of the entire flake, which clearly illustrates a nonuniform feature with a triangular core and varied layers along the base edge domain. Three representative areas (e, g, and h) were then zoomed in to reveal the detailed information as shown in Figure 3e, g, and h, respectively. After the zoom in, the periodical sapphire steps were observed simultaneously with the $WSe_2$ flake (Figure 3e and g). The direction of those steps is the same as the direction of the $WSe_2$ flake base edge, which

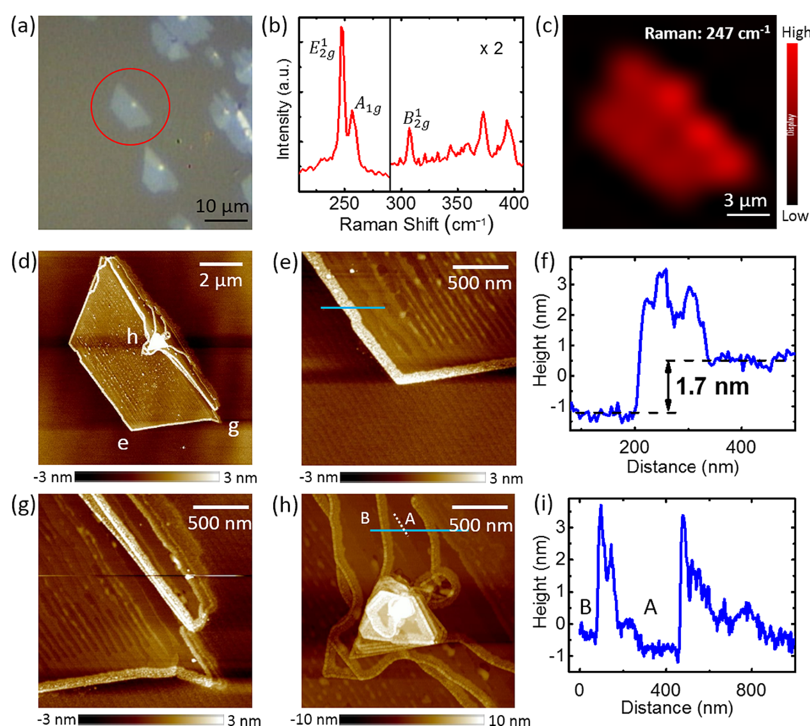


**Figure 3. Raman and AFM characterization of a typical aligned $WSe_2$ flake grown on C-plane sapphire substrates. (a) Optical image of an aligned $WSe_2$ flake with a trapezoid shape. (b) Raman spectrum of the flake in (a) showing it is a few-layer sample. The intensity is multiplied by a factor of 2 from region 300 to 400 $cm^{-1}$. (c) Raman intensity mapping of the flake in (a) at 247 $cm^{-1}$ showing nonuniform intensity over the whole flake, indicating a change of sample thickness at different locations. (d) AFM height image of the whole flake. The lateral size of this flake is about 10 $\mu$m. The areas e, g, and h are further zoomed in as shown in (e), (g), and (h), respectively. (e) Zoom-in image of the area e. The periodical sapphire step pattern is observed with a consistent direction. (f) Cross-section height profile showing the front domain of the flake is a bilayer. (g) Zoom-in image of the area g showing the detailed thickness variation along the base edge. The white dotted line indicates the base edge of layer B, which is covered by layer A. (h) Zoom-in image of the area h reveals that the core is a screw dislocation hillock as well as the layer-over-layer thickness variation. (i) Cross-section height profile along the blue line in (h).**

is consistent with the optical microscopic results. Thus, both AFM and optical observations confirm that the step direction determines the growth direction. Moreover, Figure 3g and h show that the thickness of the flake varies from the front domain to the base edge domain. The front domain is rather uniform, and it has a thickness of 1.7 nm, which can be characterized as a bilayer $WSe_2$ region. Interestingly, the sapphire step topography is well duplicated onto this bilayer region (Supporting Information Figure S5). The extra height at the flake edge is presumably due to the edge rolling effect, as also reported in the graphene study.[59] Meanwhile, Figure 3g shows more details about the thickness variation along the base edge. As we can see, the origin of the thickness variation comes from the layer-over-layer overlapping. Similar features can be found in Figure 3h as well: one layer (layer A) grows over another layer (layer B), forming a stack. However, due to the layer mismatch, such overlapping growth generates a high probability of initiating screw dislocations, which leads to a screw dislocation hillock.[60] So those "cores" along the base edges are initialized from layer-over-layer growth and developed by further screw-dislocation-driven growth. Similar screw dislocation hillocks exist in almost all the flakes (Supporting Information Figure S6). We also transferred $WSe_2$ flakes onto transmission electron microscopy (TEM) grids by a standard PMMA-mediated transfer method for high-resolution TEM (HRTEM) and diffraction studies (Supporting Information Figure S7).[61] Overall, HRTEM images show high-crystalline $WSe_2$ samples with clear hexagonal symmetry, and diffraction results suggest that the as-grown $WSe_2$ flakes are single crystals with a regular AB stacking structure.

Besides the aligned nucleation and growth phenomena we described above, the atomic steps on sapphire also have a significant effect on the few-layer $WSe_2$ formation based on our observations (Figure 3g and h) and previous studies on step-edge-guided growth of other materials.[46,49] The existence of periodic sapphire steps facilitates an aligned layer-over-layer growth during the propagation of each individual $WSe_2$ layer. Previously, the growth of few-layer TMDCs was reported to follow a traditional layer-by-layer growth mode; that is, nucleation is first formed at the preexisting bottom layer and then grown to become an additional layer (Figure 4a). In our case, the few-layer features are grown from the overlapping of individual layers. A typical model can be described as the uphill layer propagating to overlap with the downhill layer while the growth across the uphill sapphire step is

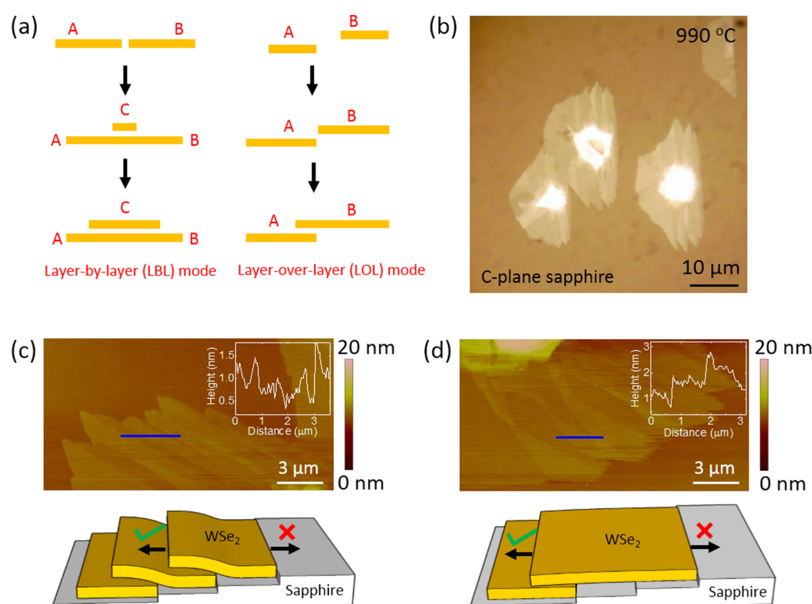


**Figure 4. Studies of the layer-over-layer (LOL) features along with proposed growth models. (a) Schematics of the layer-by-layer growth mode and layer-over-layer growth mode. (b) Optical image of as-grown $WSe_2$ flakes on C-plane sapphire at 990 °C. The domains near the base edges of these flakes evolve into a wing-like structure. (c, d) Two situations of forming few-layer $WSe_2$ by layer-over-layer overlapping of individual $WSe_2$ layers. (c) Overlapping occurs between the layers grown from adjacent steps. (d) Overlapping occurs between the layers grown from nonadjacent steps. The insets correspond to the height profiles along the blue lines in (c) and (d). The propagation across the uphill step is suppressed at high growth temperatures for both situations, leaving straight and aligned base edges.**

suppressed, leaving a straight boundary as shown in Figure 4a. This phenomenon becomes more essential at higher temperature (990 °C), as the domains near the base edge become wing-like structures (Figure 4b and Figure S1). With further AFM measurements, two kinds of overlapping were identified, as shown in Figure 4c and d. In Figure 4c, the overlapped few-layer regions have a waved structure. Since the height of a single sapphire step ($c/6$, ~0.2 nm) is less than the thickness of a monolayer of $WSe_2$ (~0.7 nm), the uphill layer has to bend when it propagates to overlap with the downhill layer generated from the adjacent step. In the other situation as shown in Figure 4d, the uphill layer will naturally fall onto the downhill layer if they are grown from nonadjacent steps showing a flat overlapped region. In addition, most of the aligned $WSe_2$ flakes in this study possess a truncated shape, which would come from the modulations of atomic steps as well. The periodic atomic steps have effects on both the front and back sides of $WSe_2$ flakes during growth. For the back side, $WSe_2$ flakes cannot climb over an uphill step, which gives a line shape base edge. For the front side, $WSe_2$ can grow downhill, but the speed of the growth front will be modulated by the atomic steps. Therefore, we observed truncated $WSe_2$ flakes with the front and base edges parallel to the direction of atomic steps on substrates. A similar phenomenon, *i.e.*, the growth of truncated graphene (can be described as lens-shaped) on a Ru substrate, was reported previously.[62] The authors stated that the formation of such lens-shaped graphene is due to the atomic steps on the Ru (0001) surface.

## CONCLUSION

In summary, we have identified a brand new mechanism for aligned growth of few-layer $WSe_2$ flakes by the CVD method using C-plane sapphire substrates. We observed that at high growth temperatures the aligned features of $WSe_2$ flakes originate from the periodical atomic steps on the sapphire surface, as supported by detailed AFM examinations. Such atomic steps on sapphire have two significant effects on the growth behavior of $WSe_2$. First, the atomic steps provide active nucleation sites to generate aligned $WSe_2$ nuclei. Second, the periodical steps lead to a layer-over-layer overlapping to form aligned few-layer $WSe_2$ flakes, which is distinct from the classical layer-by-layer mode in thin-film formation. This study not only introduces a new method for the alignment-controlled growth of 2D $WSe_2$ but also sheds light on the nucleation and growth mechanism of $WSe_2$.

## METHODS

**Step-Edge-Guided Growth of Aligned $WSe_2$ Flakes.** A CVD furnace with a one-inch quartz reaction tube was used for $WSe_2$ synthesis on either $Si/SiO_2$ or C-plane sapphire substrates. In brief, $WO_3$ powder (10 mg, Sigma-Aldrich, 99%) was placed in a ceramic boat and set at the center of the furnace. The growth substrates were sitting on top of the $WO_3$ powders and facing

down. Another boat with Se powder (15 mg, Sigma-Aldrich, 99%) was placed upstream of the furnace at a temperature of about 500 °C during growth. Ar and $H_2$ were used as carrier gases with flow rates of 80 and 20 sccm during the whole process. The furnace temperature was ramped to the growth temperature (900−990 °C) in 15 min and kept for 10 min for $WSe_2$ growth. After that, the furnace was cooled naturally under protection of 80 sccm of Ar.

**Characterization.** Raman measurements were performed with a 532 nm green laser (Renishaw Raman system with a laser spot size of around 1 $\mu$m). AFM characterization was carefully conducted to image atomic steps of C-plane sapphire substrates using a peak force tapping mode (Bruker Dimension Icon). Another AFM instrument (Digital Instrument DI 3100), SEM (Hitachi S4700, 0.5 kV or 1 kV), and TEM (JEOL 2100 F, 200 kV) were also used to image as-grown $WSe_2$ flakes.

*Conflict of Interest:* The authors declare no competing financial interest.

*Acknowledgment.* This work was supported by the Office of Naval Research (ONR) and the Air Force Office of Scientific Research (AFOSR). We would like to acknowledge the collaboration of this research with King Abdul-Aziz City for Science and Technology (KACST) *via* The Center of Excellence for Nanotechnologies (CEGN). We acknowledge Stephen Cronin of University of Southern California for access to the Raman facility and Adam Stieg of University of California, Los Angeles, for AFM measurements in California NanoSystems Institute (CNSI). TEM data presented in this article were acquired at the Center for Electron Microscopy and Microanalysis (CEMMA) at the University of Southern California.

*Supporting Information Available:* Additional SEM, Raman, PL, AFM, and TEM results. The Supporting Information is available free of charge on the ACS Publications website at DOI: 10.1021/acsnano.5b03043.

## REFERENCES AND NOTES

1. Radisavljevic, B.; Radenovic, A.; Brivio, J.; Giacometti, V.; Kis, A. Single-Layer $MoS_2$ Transistors. *Nat. Nanotechnol.* **2011**, *6*, 147–150.
2. Wang, Q. H.; Kalantar-Zadeh, K.; Kis, A.; Coleman, J. N.; Strano, M. S. Electronics and Optoelectronics of Two-Dimensional Transition Metal Dichalcogenides. *Nat. Nanotechnol.* **2012**, *7*, 699–712.
3. Wu, W.; Wang, L.; Li, Y.; Zhang, F.; Lin, L.; Niu, S.; Chenet, D.; Zhang, X.; Hao, Y.; Heinz, T. F.; *et al.* Piezoelectricity of Single-Atomic-Layer $MoS_2$ for Energy Conversion and Piezotronics. *Nature* **2014**, *514*, 470–474.
4. Li, L. K.; Yu, Y. J.; Ye, G. J.; Ge, Q. Q.; Ou, X. D.; Wu, H.; Feng, D. L.; Chen, X. H.; Zhang, Y. B. Black Phosphorus Field-Effect Transistors. *Nat. Nanotechnol.* **2014**, *9*, 372–377.
5. Liu, H.; Neal, A. T.; Zhu, Z.; Luo, Z.; Xu, X. F.; Tomanek, D.; Ye, P. D. D. Phosphorene: An Unexplored 2D Semiconductor with a High Hole Mobility. *ACS Nano* **2014**, *8*, 4033–4041.
6. Xia, F. N.; Wang, H.; Jia, Y. C. Rediscovering Black Phosphorus as an Anisotropic Layered Material for Optoelectronics and Electronics. *Nat. Commun.* **2014**, *5*, 4458.
7. Tao, L.; Cinquanta, E.; Chiappe, D.; Grazianetti, C.; Fanciulli, M.; Dubey, M.; Molle, A.; Akinwande, D. Silicene Field-Effect Transistors Operating at Room Temperature. *Nat. Nanotechnol.* **2015**, *10*, 227–231.
8. Pu, J.; Yomogida, Y.; Liu, K. K.; Li, L. J.; Iwasa, Y.; Takenobu, T. Highly Flexible $MoS_2$ Thin-Film Transistors with Ion Gel Dielectrics. *Nano Lett.* **2012**, *12*, 4013–4017.
9. Chang, H. Y.; Yang, S. X.; Lee, J. H.; Tao, L.; Hwang, W. S.; Jena, D.; Lu, N. S.; Akinwande, D. High-Performance, Highly Bendable $MoS_2$ Transistors with High-*K* Dielectrics for Flexible Low-Power Systems. *ACS Nano* **2013**, *7*, 5446–5452.
10. Akinwande, D.; Petrone, N.; Hone, J. Two-Dimensional Flexible Nanoelectronics. *Nat. Commun.* **2014**, *5*, 5678.
11. Baugher, B. W. H.; Churchill, H. O. H.; Yang, Y. F.; Jarillo-Herrero, P. Optoelectronic Devices Based on Electrically Tunable P-N Diodes in a Monolayer Dichalcogenide. *Nat. Nanotechnol.* **2014**, *9*, 262–267.
12. Pospischil, A.; Furchi, M. M.; Mueller, T. Solar-Energy Conversion and Light Emission in an Atomic Monolayer P-N Diode. *Nat. Nanotechnol.* **2014**, *9*, 257–261.
13. Ross, J. S.; Klement, P.; Jones, A. M.; Ghimire, N. J.; Yan, J.; Mandrus, D. G.; Taniguchi, T.; Watanabe, K.; Kitamura, K.; Yao, W.; *et al.* Electrically Tunable Excitonic Light-Emitting Diodes Based on Monolayer $WSe_2$ P-N Junctions. *Nat. Nanotechnol.* **2014**, *9*, 268–272.
14. Desai, S. B.; Seol, G.; Kang, J. S.; Fang, H.; Battaglia, C.; Kapadia, R.; Ager, J. W.; Guo, J.; Javey, A. Strain-Induced Indirect to Direct Bandgap Transition in Multilayer $WSe_2$. *Nano Lett.* **2014**, *14*, 4592–4597.
15. Yin, Z.; Li, H.; Li, H.; Jiang, L.; Shi, Y.; Sun, Y.; Lu, G.; Zhang, Q.; Chen, X.; Zhang, H. Single-Layer $MoS_2$ Phototransistors. *ACS Nano* **2012**, *6*, 74–80.
16. Mak, K. F.; He, K. L.; Shan, J.; Heinz, T. F. Control of Valley Polarization in Monolayer $MoS_2$ by Optical Helicity. *Nat. Nanotechnol.* **2012**, *7*, 494–498.
17. Perkins, F. K.; Friedman, A. L.; Cobas, E.; Campbell, P. M.; Jernigan, G. G.; Jonker, B. T. Chemical Vapor Sensing with Monolayer $MoS_2$. *Nano Lett.* **2013**, *13*, 668–673.
18. Voiry, D.; Yamaguchi, H.; Li, J.; Silva, R.; Alves, D. C. B.; Fujita, T.; Chen, M.; Asefa, T.; Shenoy, V. B.; Eda, G.; *et al.* Enhanced Catalytic Activity in Strained Chemically Exfoliated $WS_2$ Nanosheets for Hydrogen Evolution. *Nat. Mater.* **2013**, *12*, 850–855.
19. Liu, B.; Chen, L.; Liu, G.; Abbas, A. N.; Fathi, M.; Zhou, C. High-Performance Chemical Sensing Using Schottky-Contacted Chemical Vapor Deposition Grown Monolayer $MoS_2$ Transistors. *ACS Nano* **2014**, *8*, 5304–5314.
20. Wang, H.; Yu, L.; Lee, Y.; Shi, Y.; Hsu, A.; Chin, M. L.; Li, L.; Dubey, M.; Kong, J.; Palacios, T. Integrated Circuits Based on Bilayer $MoS_2$ Transistors. *Nano Lett.* **2012**, *12*, 4674–4680.
21. Tosun, M.; Chuang, S.; Fang, H.; Sachid, A. B.; Hettick, M.; Lin, Y. J.; Zeng, Y. P.; Javey, A. High-Gain Inverters Based on $WSe_2$ Complementary Field-Effect Transistors. *ACS Nano* **2014**, *8*, 4948–4953.
22. Butler, S. Z.; Hollen, S. M.; Cao, L.; Cui, Y.; Gupta, J. A.; Gutierrez, H. R.; Heinz, T. F.; Hong, S. S.; Huang, J.; Ismach, A. F.; *et al.* Progress, Challenges, and Opportunities in Two-Dimensional Materials Beyond Graphene. *ACS Nano* **2013**, *7*, 2898–2926.
23. Li, H.; Lu, G.; Wang, Y.; Yin, Z.; Cong, C.; He, Q.; Wang, L.; Ding, F.; Yu, T.; Zhang, H. Mechanical Exfoliation and Characterization of Single- and Few-Layer Nanosheets of $WSe_2$, $TaS_2$, and $TaSe_2$. *Small* **2013**, *9*, 1974–1981.
24. Novoselov, K. S.; Jiang, D.; Schedin, F.; Booth, T. J.; Khotkevich, V. V.; Morozov, S. V.; Geim, A. K. Two-Dimensional Atomic Crystals. *Proc. Natl. Acad. Sci. U. S. A.* **2005**, *102*, 10451–10453.
25. Chhowalla, M.; Shin, H. S.; Eda, G.; Li, L. J.; Loh, K. P.; Zhang, H. The Chemistry of Two-Dimensional Layered Transition Metal Dichalcogenide Nanosheets. *Nat. Chem.* **2013**, *5*, 263–275.
26. Green, A. A.; Hersam, M. C. Solution Phase Production of Graphene with Controlled Thickness Via Density Differentiation. *Nano Lett.* **2009**, *9*, 4031–4036.
27. Coleman, J. N.; Lotya, M.; O'Neill, A.; Bergin, S. D.; King, P. J.; Khan, U.; Young, K.; Gaucher, A.; De, S.; Smith, R. J.; *et al.* Two-Dimensional Nanosheets Produced by Liquid Exfoliation of Layered Materials. *Science* **2011**, *331*, 568–571.
28. Huang, J. K.; Pu, J.; Hsu, C.; Chiu, M.; Juang, Z.; Chang, Y.; Chang, W.; Iwasa, Y.; Takenobu, T.; Li, L. Large-Area Synthesis of Highly Crystalline $WSe_2$ Mono Layers and Device Applications. *ACS Nano* **2014**, *8*, 923–930.
29. Zhou, H. L.; Wang, C.; Shaw, J. C.; Cheng, R.; Chen, Y.; Huang, X.; Liu, Y.; Weiss, N. O.; Lin, Z.; Huang, Y.; *et al.* Large Area Growth and Electrical Properties of p-Type $WSe_2$ Atomic Layers. *Nano Lett.* **2015**, *15*, 709–713.
30. Eichfeld, S. M.; Hossain, L.; Lin, Y.; Piasecki, A. F.; Kupp, B.; Birdwell, A. G.; Burke, R. A.; Lu, N.; Peng, X.; Li, J.; *et al.* Highly Scalable, Atomically Thin $WSe_2$ Grown Via Metal-Organic

Chemical Vapor Deposition. *ACS Nano* **2015**, *9*, 2080–2087.

31. Wang, X.; Gong, Y.; Shi, G.; Chow, W. L.; Keyshar, K.; Ye, G.; Vajtai, R.; Lou, J.; Liu, Z.; Ringe, E.; *et al*. Chemical Vapor Deposition Growth of Crystalline Monolayer $MoSe_2$. *ACS Nano* **2014**, *8*, 5125–5131.
32. Zhang, Y.; Ji, Q.; Han, G.; Ju, J.; Shi, J.; Ma, D.; Sun, J.; Zhang, Y.; Li, M.; Lang, X.; *et al*. Dendritic, Transferable, Strictly Monolayer $MoS_2$ Flakes Synthesized on $SrTiO_3$ Single Crystals for Efficient Electrocatalytic Applications. *ACS Nano* **2014**, *8*, 8617–8624.
33. Ling, X.; Lee, Y. H.; Lin, Y.; Fang, W.; Yu, L.; Dresselhaus, M. S.; Kong, J. Role of the Seeding Promoter in $MoS_2$ Growth by Chemical Vapor Deposition. *Nano Lett.* **2014**, *14*, 464–472.
34. Chen, Y. Z.; Medina, H.; Su, T. Y.; Li, J. G.; Cheng, K. Y.; Chiu, P. W.; Chueh, Y. L. Ultrafast and Low Temperature Synthesis of Highly Crystalline and Patternable Few-Layers Tungsten Diselenide by Laser Irradiation Assisted Selenization Process. *ACS Nano* **2015**, *9*, 4346–4353.
35. Liu, B.; Fathi, M.; Chen, L.; Abbas, A.; Ma, Y.; Zhou, C. W. Chemical Vapor Deposition Growth of Monolayer $WSe_2$ with Tunable Device Characteristics and Growth Mechanism Study. *ACS Nano* **2015**, *9*, 6119–6127.
36. Ma, Y.; Liu, B.; Zhang, A.; Chen, L.; Fathi, M.; Shen, C.; Abbas, A.; Ge, M.; Mecklenburg, M.; Zhou, C. W. Reversible Semiconducting-to-Metallic Phase Transition in Chemical Vapor Deposition Grown Monolayer $WSe_2$ and Applications for Devices. *ACS Nano* **2015**, *9*, 7383–7391.
37. Clark, G.; Wu, S. F.; Rivera, P.; Finney, J.; Nguyen, P.; Cobden, D. H.; Xu, X. D. Vapor-Transport Growth of High Optical Quality $WSe_2$ Monolayers. *APL Mater.* **2014**, *2*.101101
38. van der Zande, A. M.; Huang, P. Y.; Chenet, D. A.; Berkelbach, T. C.; You, Y.; Lee, G.; Heinz, T. F.; Reichman, D. R.; Muller, D. A.; Hong, J. C. Grains and Grain Boundaries in Highly Crystalline Monolayer Molybdenum Disulphide. *Nat. Mater.* **2013**, *12*, 554–561.
39. Lu, X.; Utama, M. I. B.; Lin, J.; Gong, X.; Zhang, J.; Zhao, Y.; Pantelides, S. T.; Wang, J.; Dong, Z.; Liu, Z.; *et al*. Large-Area Synthesis of Monolayer and Few-Layer $MoSe_2$ Films on $SiO_2$ Substrates. *Nano Lett.* **2014**, *14*, 2419–2425.
40. Cong, C. X.; Shang, J. Z.; Wu, X.; Cao, B. C.; Peimyoo, N.; Qiu, C.; Sun, L. T.; Yu, T. Synthesis and Optical Properties of Large-Area Single-Crystalline 2D Semiconductor $WS_2$ Monolayer from Chemical Vapor Deposition. *Adv. Opt. Mater.* **2014**, *2*, 131–136.
41. Kang, K.; Xie, S.; Huang, L.; Han, Y.; Huang, P. Y.; Mak, K. F.; Kim, C. J.; Muller, D.; Park, J. High-Mobility Three-Atom-Thick Semiconducting Films with Wafer-Scale Homogeneity. *Nature* **2015**, *520*, 656–660.
42. Lee, J. H.; Lee, E. K.; Joo, W. J.; Jang, Y.; Kim, B. S.; Lim, J. Y.; Choi, S. H.; Ahn, S. J.; Ahn, J. R.; Park, M. H.; *et al*. Wafer-Scale Growth of Single-Crystal Monolayer Graphene on Reusable Hydrogen-Terminated Germanium. *Science* **2014**, *344*, 286–289.
43. Han, G. H.; Kybert, N. J.; Naylor, C. H.; Lee, B. S.; Ping, J.; Park, J. H.; Kang, J.; Lee, S. Y.; Lee, Y. H.; Agarwal, R.; *et al*. Seeded Growth of Highly Crystalline Molybdenum Disulphide Monolayers at Controlled Locations. *Nat. Commun.* **2015**, *6*, 6128.
44. Dumcenco, D.; Ovchinnikov, D.; Marinov, K.; Lopez-Sanchez, O.; Krasnozhon, D.; Chen, M.; Gillet, P.; Morral, A. F. I; Radenovic, A.; Kis, A.; *et al*. Large-Area Epitaxial Monolayer $MoS_2$. *ACS Nano* **2015**, *9*, 4611–4620.
45. Ji, Q. Q.; Zhang, Y.; Gao, T.; Zhang, Y.; Ma, D.; Liu, M.; Chen, Y.; Qiao, X.; Tan, P.; Kan, M.; *et al*. Epitaxial Monolayer $MoS_2$ on Mica with Novel Photoluminescence. *Nano Lett.* **2013**, *13*, 3870–3877.
46. Ismach, A.; Segev, L.; Wachtel, E.; Joselevich, E. Atomic-Step-Templated Formation of Single Wall Carbon Nanotube Patterns. *Angew. Chem., Int. Ed.* **2004**, *43*, 6140–6143.
47. Han, S.; Liu, X. L.; Zhou, C. W. Template-Free Directional Growth of Single-Walled Carbon Nanotubes on a- and R-Plane Sapphire. *J. Am. Chem. Soc.* **2005**, *127*, 5294–5295.
48. Kocabas, C.; Hur, S. H.; Gaur, A.; Meitl, M. A.; Shim, M.; Rogers, J. A. Guided Growth of Large-Scale, Horizontally Aligned Arrays of Single-Walled Carbon Nanotubes and Their Use in Thin-Film Transistors. *Small* **2005**, *1*, 1110–1116.
49. Tsivion, D.; Schvartzman, M.; Popovitz-Biro, R.; von Huth, P.; Joselevich, E. Guided Growth of Millimeter-Long Horizontal Nanowires with Controlled Orientations. *Science* **2011**, *333*, 1003–1007.
50. Kurnosikov, O.; Van, L. P.; Cousty, J. About Anisotropy of Atomic-Scale Height Step on (0001) Sapphire Surface. *Surf. Sci.* **2000**, *459*, 256–264.
51. Heffelfinger, J. R.; Bench, M. W.; Carter, C. B. Steps and the Structure of the (0001) Alpha-Alumina Surface. *Surf. Sci.* **1997**, *370*, L168–L172.
52. Yan, K.; Peng, H. L.; Zhou, Y.; Li, H.; Liu, Z. F. Formation of Bilayer Bernal Graphene: Layer-by-Layer Epitaxy *via* Chemical Vapor Deposition. *Nano Lett.* **2011**, *11*, 1106–1110.
53. Zhang, Y.; Zhang, L. Y.; Kim, P.; Ge, M. Y.; Li, Z.; Zhou, C. W. Vapor Trapping Growth of Single-Crystalline Graphene Flowers: Synthesis, Morphology, and Electronic Properties. *Nano Lett.* **2012**, *12*, 2810–2816.
54. Saadi, S.; Abild-Pedersen, F.; Helveg, S.; Sehested, J.; Hinnemann, B.; Appel, C. C.; Norskov, J. K. On the Role of Metal Step-Edges in Graphene Growth. *J. Phys. Chem. C* **2010**, *114*, 11221–11227.
55. Geblinger, N.; Ismach, A.; Joselevich, E. Self-Organized Nanotube Serpentines. *Nat. Nanotechnol.* **2008**, *3*, 195–200.
56. Liu, B. L.; Wang, C.; Liu, J.; Che, Y. C.; Zhou, C. W. Aligned Carbon Nanotubes: From Controlled Synthesis to Electronic Applications. *Nanoscale* **2013**, *5*, 9483–9502.
57. Somorjai, G. A. Modern Surface Science and Surface Technologies: An Introduction. *Chem. Rev.* **1996**, *96*, 1223–1235.
58. Wang, S.; Rong, Y.; Fan, Y.; Pacios, M.; Bhaskaran, H.; He, K.; Warner, J. H. Shape Evolution of Monolayer MoS2 Crystals Grown by Chemical Vapor Deposition. *Chem. Mater.* **2014**, *26*, 6371–6379.
59. Gao, L. B.; Ren, W. C.; Liu, B. L.; Saito, R.; Wu, Z. S.; Li, S. S.; Jiang, C. B.; Li, F.; Cheng, H. M. Surface and Interference Coenhanced Raman Scattering of Graphene. *ACS Nano* **2009**, *3*, 933–939.
60. Chen, L.; Liu, B. L.; Abbas, A. N.; Ma, Y. Q.; Fang, X.; Liu, Y. H.; Zhou, C. W. Screw-Dislocation-Driven Growth of Two-Dimensional Few-Layer and Pyramid-Like $WSe_2$ by Sulfur-Assisted Chemical Vapor Deposition. *ACS Nano* **2014**, *8*, 11543–11551.
61. Liu, B.; Ren, W.; Gao, L.; Li, S.; Pei, S.; Liu, C.; Jiang, C.; Cheng, H. M. Metal-Catalyst-Free Growth of Single-Walled Carbon Nanotubes. *J. Am. Chem. Soc.* **2009**, *131*, 2082–2083.
62. Sutter, P. W.; Flege, J. I.; Sutter, E. A. Epitaxial Graphene on Ruthenium. *Nat. Mater.* **2008**, *7*, 406–411.